Heterogenization of photochemical molecular devices: embedding metal-organic cage into ZIF-8-derived matrix to promote proton and electron transfer

Journal:	*Journal of the American Chemical Society*
Manuscript ID	ja-2019-03981f.R1
Manuscript Type:	Article
Date Submitted by the Author:	28-Jun-2019
Complete List of Authors:	Luo , Yu-Cheng ; Sun Yat-Sen University, School of Chemistry Chu, Kun-Ling ; Sun Yat-Sen University, School of Chemistry Shi, Jian-Ying; Sun Yat-Sen University, School of Chemistry Wu, Dong-Jun ; Sun Yat-Sen University, School of Chemistry Wang, Xu-Dong; Sun Yat-Sen University Mayor, Marcel; Universitat Basel, Department of Chemistry; Sun Yat-Sen University, Lehn Institute of Functional Materials, School of Chemistry Su, Cheng-Yong; Sun Yat-Sen University, School of Chemistry

Heterogenization of photochemical molecular devices: embedding metal-organic cage into ZIF-8-derived matrix to promote proton and electron transfer

Yu-Cheng Luo[1], Kun-Ling Chu[1], Jian-Ying Shi[1]*, Dong-Jun Wu[1], Xu-Dong Wang[1], Marcel Mayor[1] and Cheng-Yong Su[1,2]*

[1]MOE Laboratory of Bioinorganic and Synthetic Chemistry, Lehn Institute of Functional Materials, School of Chemistry, Sun Yat-Sen University, Guangzhou 510275, China.

[2]State Key Laboratory of Organometallic Chemistry, Shanghai Institute of Organic Chemistry, Chinese Academy of Sciences, Shanghai 200032, China.

Keywords: *heterogenous catalyst, metal-organic cage, photochemical molecular device, H_2 production, photocatalysis*

ABSTRACT: Application of molecular catalyst in artificial photosynthesis is confronted with challenges like rapid deactivation due to photodegradation or detrimental aggregation in harsh conditions. In this work, a metal-organic cage $[Pd_6(RuL_3)_8]^{28+}$ (MOC-16), characteristic of a photochemical molecular device (PMD) concurrently integrating eight Ru^{2+} light-harvesting centers and six Pd^{2+} catalytic centers for efficient homogeneous H_2 production, is successfully heterogenized through incorporation into a metal-organic framework (MOF) of ZIF-8, and then transformed into a carbonate matrix of $Zn_x(MeIm)_x(CO_3)_x$ (CZIF) to lead to hybridized MOC-16@CZIF. This MOC@MOF integrated photocatalyst inherits the highly efficient and directional electron transfer in picosecond domain of MOC-16, and possesses one order increased microsecond magnitude of the triplet excited-state electron in comparison to the primitive MOC-16. The carbonate CZIF-matrix endows MOC-16@CZIF with water-wettability, serving as proton relay to facilitate proton delivery by virtue of H_2O as proton carriers. The electron transfer during photocatalytic process is also enhanced by infiltration of sacrificial agent of BIH into CZIF-matrix to promote conductivity, owing to its strong reducing ability to induce free charge carriers. These synergistic effects contribute to the extra high activity for H_2 generation, making the turnover frequency of this heterogeneous MOC-16@CZIF photocatalyst maintain a level of ~0.4 $H_2 \cdot s^{-1}$, increased by 50-fold than homogenous PMD. Meanwhile, it is robust enough to tolerate harsh reaction conditions, presenting an unprecedented heterogenization example of homogeneous PMD with MOF-derived matrix to mimic catalytic feature of nature photosystem, which may shed a light on the design of multifunctional PMD@MOF materials to expand plenty of molecular catalysts to practical application in artificial photosynthesis.

INTRODUCTION

Artificial photosynthesis, taking nature as an example by manipulating light-harvesting antennae and catalytic centers to fulfil solar-to-fuel conversion directly and efficiently, provides an attractive solution for large-scale energy storage and usage.[1-3] Photochemical molecular devices (PMDs), organizing chromophoric photosensitizer, catalytic center and electron relay in a molecular level, is competent for efficient electron and energy transfer in photocatalysis, reminiscent of collaborative and synergistic functions in photosystems I and II.[4-8] However, the development of PMDs for practical applications still faces challenges including: (1) proper organization of multiple photosensitizing and catalytic centers in one PMD while maintaining efficient and directional electron transfer, since at least two electrons have to be consumed in H_2 formation, and (2) circumventing the vulnerability of molecular catalysts under harsh photocatalytic conditions. We have developed a bimetallic $[Pd_6(RuL_3)_8]^{28+}$ (L = 2-(pyridin-3-yl)-1H-imidazo [4,5-f][1,10]-phenanthroline) metal-organic cage (MOC-16) as a new type of PMDs to unify multiple photosensitizing, electron relay and catalytic units in a highly symmetrical way to achieve directional and independent multichannel electron transfer for efficient H_2 generation;[5,9] nevertheless, photodegradation and detrimental aggregation of dissociated Pd particles after a long-time irradiation is still inevitable in homogenous photocatalysis.

Another strategy of artificial photosynthesis is based on heterogeneous catalysts, of which metal-organic frameworks (MOFs) with merits of structural regularity and synthetic tunability provide a versatile platform to hierarchically organize light-harvesting antennae and/or catalytic centers by virtue of purposely engineering coordination chemical nanospace.[10-12] Various molecular catalysts and/or photosensitizers have been integrating into MOFs as inorganic nodes, organic linkers or included guests for water photosplitting,[13,14] CO_2 photofixation and organic photosynthesis.[15] For example, by utilizing free $Ru(bpy)_3^{2+}$ as photosensitizer, Mn-bipyridine or $[Fe_2S_2]$

Scheme 1. The process to incorporate MOC-16 into ZIF-8 matrix via coordination-assisted secondary assembly followed by transforming ZIF-8 structure to CZIF-matrix in the presence of CO_2 and water.

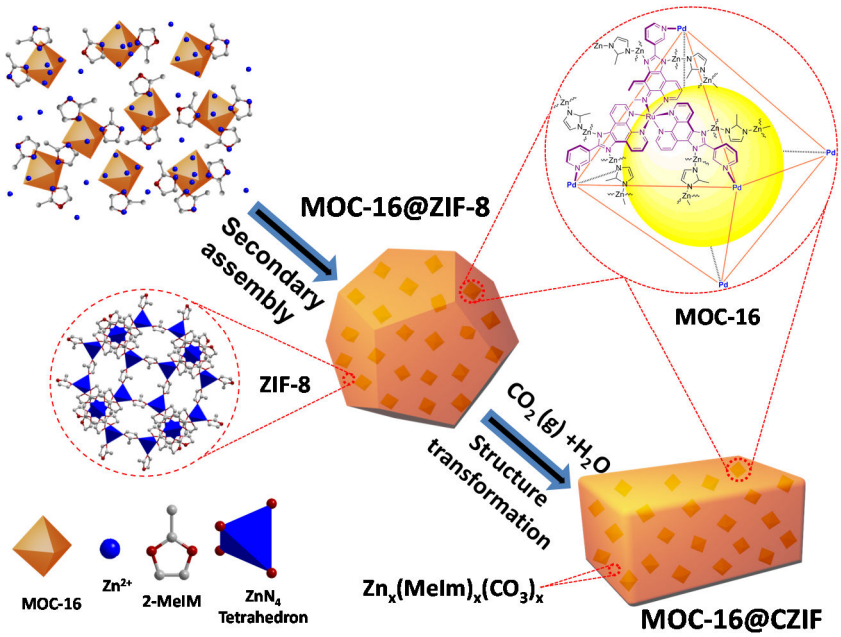

based catalysts were anchored onto organic linker of UiO-MOF for proton and CO_2 reduction.[16,17] Moreover, cobaloxime catalyst was incorporated into photo-active NH_2-MIL-125(Ti),[18] Pt-nanoparticles (Pt-NPs) were encapsulated into cavities of light-harvesting $[Ir(ppy)_2(bpy)]^+$-derived UiO-MOF,[19] and a molecular Pt^{2+} catalyst and an Ir(III) light-absorber were simultaneously embedded in UiO-MOF struts.[20] These MOF-derived catalysts did show good photoreduction activity compared with their homogenous counterparts, as a result of promoted electron transfer from guest-to-strut,[16,17] strut-to-guest,[18,19] or strut-to-strut,[20] but the photoactive centers and the catalytic centers in MOFs are still separated in space and long distance energy migration/electron hopping is challenging due to weak electronic coupling. To overcome these problems, an alternative strategy is to integrate a PMD as whole, which features close vicinity and intramolecular electron transfer between directly bonded photosensitizing and reactive centers, into MOF-matrix to facilitate efficient electron and/or energy transfers for photocatalysis. However, thus far, this type of PMD@MOF photocatalysts remain unexplored. Only resembling examples for proton reduction were found from porphyrin-derived MOFs.[21,22]

Since the MOC-type PMD takes an advantage to be able to unify multiple photosensitizing and catalytic units with efficient and directional electron transfer for homogeneous photocatalysis,[5] we envision that integrating such MOCs into an MOF-matrix could, on one hand, inherit the distinctive photocatalytic feature and, on the other hand, provide a promising strategy to heterogenize PMDs for hetereogeneous photocatalysis to tolerate harsh conditions. Moreover, the MOC@MOF integration may provide a way to adjust electron transfer dynamics via the structural and spatial heterogeneity. The microenvironments in MOF-matrix may also be able to facilitate proton transfer, provide local pH buffering, regulate ion transport, stabilize catalytic site, and so on, reminiscent of enzymatic-type behaviors.[23,]

Herein, we report a heterogenous PMD@MOF photocatalyst generated by incorporating MOC-16 into a crystalline carbonate $Zn_x(MeIm)_x(CO_3)_x$ (defined as CZIF) matrix which is in-situ derived from ZIF-8 in presence of CO_2 and water. As expected, the heterogenization imparts the embedded MOC-16 PMDs with excellent stability, while retaining high-efficient energy and electron transfer. The CZIF-matrix also engenders hydrophilic nature for proton transfer, and prolongs electron lifetime in excited-states, leading to a synergistic effect for 50-fold improvement of turnover frequency (TOF) in contrast to homogenous MOC-16 in photocatalytic H_2 generation.

RESULTS AND DISCUSSION

Design strategy. As mentioned above, the synthetic methods to incorporate molecular catalysts and/or photosensitizers into MOFs have been vigorously explored in recent years, including the mixed-ligand multivariate approach (MTV), postsynthetic exchange (PSE), sequent postsynthetic metalation (PSM),[16-18,20,21,24] as well as recent Lin`s work by directly incorporating catalyst in the secondary building units (SBUs) of photosensitizing MOFs.[22] These heterogenization approaches are usually applicable to molecular catalysts and/or photosensitizers with small size. By contrast, MOC-16 comprises eight RuL_3 photosensitizers and six Pd^{2+} catalytic centers to form huge $[Pd_6(RuL_3)_8]^{28+}$ octahedral cage with the diameter of ~3 nm and a cavity of 5350 $Å^3$.[9] Therefore, the post-modification or "ship-in-a-bottle" strategies to introduce MOCs into MOF-matrix is infeasible as limited by the pore size. Alternatively, a "bottle-around-a-ship" strategy, namely, secondary assembly of MOF on MOC outside surface, is more prone to realize their integration, analogous to our previous intercalation of $Au_{25}(SG)_{18}$ into ZIF-8 scaffolds.[25] A synthetic process of heterogenizing MOC-16 through coordination-assisted secondary assembly is illustrated in scheme 1, where MOC-16@ZIF-8 precursors are initially grown from a mixture of MOC-16, Zn^{2+} and 2-MeIm subcomponents by

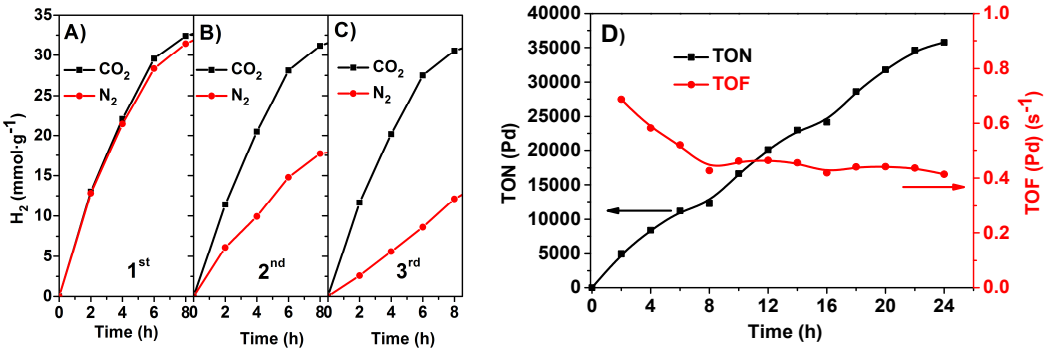

Figure 1. H_2 evolution curves with prolonging irradiation time for MOC-16@CZIF photocatalyst under N_2 and CO_2 atmosphere. A) first cycle run; B) second cycle run; C) third cycle run, and D) accumulated TONs and TOFs based on Pd-center in catalyst durability test over 24 h under CO_2 atmosphere. TON = $n(H_2)/n(Pd)$, TOF = $d_{(TON)}/d_t$. Visible-light (λ > 420 nm) irradiating with 100 mW/cm^2 intensity.

virtue of Zn-N coordination linkage between the imidazole rings of MOC-16 and the 2-MeIm ligands. Such MOC-16@ZIF-8 precursors are apt to aggregate via epitaxial growth or oriented attachment, induced by surface intension, to lead to crystallization of hybridized MOC@MOF.[26,27] Since ZIF-8 crystals are known reactive to CO_2 under moisture or liquid water conditions to cause chemical degradation,[28] a following in-situ structural transformation of ZIF-8 from $Zn(MeIm)_2$ to carbonate $Zn(MeIm)_2{\cdot}Zn(CO_3)_2{\cdot}0.66HMeIM$ (CZIF) in the presence of H_2O and CO_2 is carried out, finally giving rise to MOC-16@CZIF. This transformation from ZIF-8 to carbonate CZIF has been reported to originate from partial substitution of MeIm by CO_3^{2-} carbonate,[28] while the integrated MOC-16 in the CZIF scaffold is well retained.

H_2 production. The photocatalytic H_2 evolution has been evaluated by visible light irradiation (λ > 420 nm) in the presence of sacrificial agent of 1,3-dimethyl-2-phenyl-2,3-dihydro-1H-benzimidazole (BIH) in a mixed solvent of H_2O and MeCN (v/v = 2/3) under N_2 or CO_2 atmosphere. For the pristine MOC-16@ZIF-8 catalyst, only trace H_2 is detected under N_2 atmosphere; however, remarkable H_2 evolution is observed in the presence of CO_2 (Figure S1). The X-ray diffraction (XRD) structural characterization of the recovered catalyst indicates that ZIF-8 matrix in MOC-16@ZIF-8 has been simultaneously transformed to CZIF in photocatalytic process, which is consistent with the literature that ZIF-8 is sensitive to CO_2 in H_2O environment.[28] Therefore, prior to photocatalytic reaction, the pristine MOC-16@ZIF-8 was changed to MOC-16@CZIF to evaluate the H_2 generation performance. As shown in Figure 1, almost same H_2 evolution curves are obtained under N_2 and CO_2 atmosphere for MOC-16@CZIF. The H_2 output after 8 h reaches up to ~32 mmol·g^{-1}, corresponding to complete consumption of BIH as a one-electron donor. The accumulated turnover number (TON) based on Pd-centers is ~12317 in 8 h, and the instantaneous TOF at 8 h is estimated for 0.43 H_2 s^{-1}, both of them are far higher than homogenous MOC-16 system of 635 (48 h) and 30 H_2 h^{-1} in our previous work.[5] Table S1 summarizes the H_2 generation results under various experimental conditions over 8 h irradiation, in together with the control experimental results. In the absence of MOC-16 or BIH (entries 5 and 6), no H_2 evolution is detected, confirming that the PMD of MOC-16 and sacrificial agent are indispensable for H_2 generation. The light on/off curve further indicates that H_2 evolution is a photochemical process initiated with light irradiation (Figure S2). The dosages for the photocatalyst and BIH are optimized as shown Figure S3, indicating a preferable catalytic condition: 1 mg MOC-16@CZIF photocatalyst in 5 mL H_2O-MeCN (v/v = 2/3) mixture containing 14 mg sacrificial agent of BIH. It should be mentioned that only minimal amount of CO and HCOOH is detected for MOC-16@CZIF catalyst after 8 h light-irradiation (Table S1), irrespective of CO_2 or N_2 atmosphere and H_2O presence. These results indicate that MOC-16@CZIF is not competent for CO_2 reduction, thereof showing high H_2 evolution selectivity. It is also noticeable that, although a basic solvent mixture of DMSO/H_2O with TEOA as sacrificial agent is preferred for the homogeneous H_2 production with MOC-16,[5] a slightly acidic reaction condition in presence of CO_2 is generated (pH ~ 6) in present case, which makes BIH as a more suitable sacrificial agent in heterogeneous system MOC-16@CZIF. On the contrary, with BIH as sacrificial agent without protection of CZIF-matrix, the MOC-16 homogenous photocatalyst is apt to reduction to black Pd in solution, leading to ineffectiveness of H_2 evolution (Figure S4).

To test the catalytic durability of the resulting heterogenous MOC-16@CZIF photocatalyst, the sequential reaction-cycles (8 h per cycle) were carried out under both CO_2 and N_2 atmosphere. As seen from Figure 1, the comparable H_2 amount is detected in three cycles under CO_2 atmosphere. By contrast, under N_2 atmosphere, H_2 production falls obviously by almost half in the second run (Figure 1B) and even less in the third run (Figure 1C), although nearly identical H_2 evolution is observed in the first cycle as that under CO_2 atmosphere (Figure 1A). This means that the presence of CO_2 plays an important role to sustain the photocatalytic performance of MOC-16@CZIF. Under CO_2 atmosphere, the accumulated TON based on Pd-center in durability test over 24 h approaches ~35000, and the instantaneous TOF_{Pd} reaches up to ~0.7 s^{-1} at beginning and then maintains at ~0.4 s^{-1} (Figure 1D).

Mechanism study. A series of controlled experiments have been carried out to unveil photocatalytic nature for H_2 evolution under comparable conditions, as depicted in Figure S4. The fragmental analogues of MOC-16, RuL_3 and $PdPy_4$ (Py = Pyridine), were concomitantly embedded into

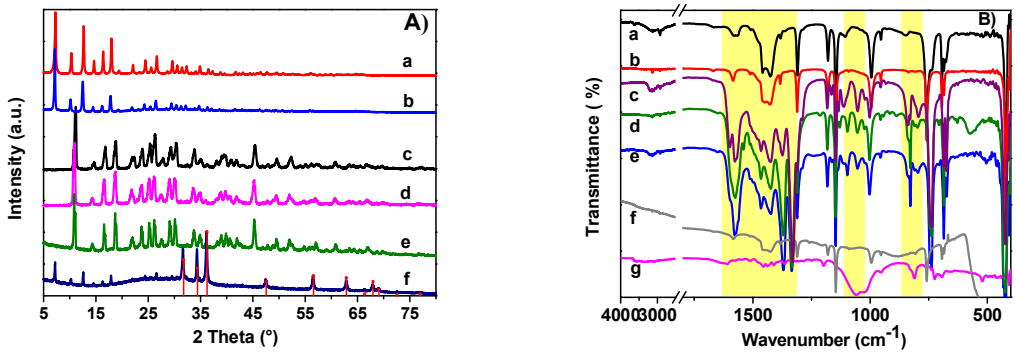

Figure 2. A) XRD patterns and B) IR spectra of MOC-16@MOF photocatalysts. From top to bottom: a) ZIF-8, b) MOC-16@ZIF-8, c) CZIF, d) MOC-16@CZIF, e) recycled MOC-16@CZIF under CO_2 atmosphere, f) recycled MOC-16@CZIF under N_2 atmosphere and g) MOC-16.

ZIF-8 matrix to give (RuL_3+$PdPy_4$)@ZIF-8, or separately incorporated into ZIF-8 matrix in combination with homogeneous $PdPy_4$ and RuL_3 to lead to $PdPy_4$@ZIF-8+RuL_3 and RuL_3@ZIF-8+$PdPy_4$ systems, respectively. It is found that, under CO_2 atmosphere, when catalytic $PdPy_4$ is embedded in MOF-matrix, H_2 generation is achieved, no matter photosensitizer RuL_3 is homogeneously dissolved into solvent or heterogeneously embedded into matrix, but lower than half amount of MOC-16@CZIF. For sample of RuL_3@matrix combining homogenous $PdPy_4$, no H_2 evolution is detected. In addition, once MOC-16@CZIF is treated with $NaBH_4$ to reduce Pd^{2+} to Pd^0 (verified by XPS in Figure S5), negligible H_2 is detectable in 8 h irradiation. These control experimental results verify that integration of whole MOC-16 as a PMD unit comprising both photosensitizing RuL_3 and catalytic $PdPy_4$ fragments is indispensable for the high activity of H_2 evolution. The intact MOC-16 structure integrated inside carbonate CZIF has also been confirmed by ^1H NMR measurement (Figure S5), where a set of proton peaks belonging to MOC-16 is detected after digesting MOC-16@CZIF.

XRD and Fourier-transform infrared (FTIR) spectra were carried out to characterize structure of heterogenous MOC@MOF catalysts before and after photocatalysis. As shown in Figure 2A, the XRD pattern of synthesized ZIF-8 matches well with literature result.[29,30] After encapsulating MOC-16 into ZIF-8, the diffraction patterns keep salient and unchanged, indicating good crystallinity of ZIF-8 matrix after integration. The structure transformation of ZIF-8 when treated with H_2O and CO_2 is evident from the well matching profile with the known carbonate CZIF,[28] which is reported to arise from partial substitution of MeIm by CO_3^{2-}. Similarly, when treating MOC-16@ZIF-8 hybrid with H_2O and CO_2, the structural conversion to MOC-16@CZIF is convincing from the identical XRD patterns with CZIF. The recycled MOC-16@CZIF catalyst under CO_2 atmosphere retains CZIF-matrix. By contrast, the recycled catalyst under N_2 atmosphere degrades to a mixture of ZIF-8 and ZnO (#36-1451), suggesting dissociation of CO_3^{2-} from CZIF-matrix in the absence of CO_2 feeding. This finding indicates that CO_2 is demanding to maintain $Zn_x(MeIm)_x(CO_3)_x$ structure. Furthermore, when comparing ZIF-8 with CZIF, or, MOC-16@ZIF-8 with MOC-16@CZIF, obvious variations of IR spectra at 750-850, 1000-1100 and 1300-1650 cm^{-1} regions are observed (Figure 2B), which are related to carbonate in CZIF as summarized in Table S2. For recycled MOC-16@CZIF-8 under CO_2 atmosphere, IR bands are analogous to those of MOC-16@CZIF, in contrast, recycled MOC-16@CZIF-8 under N_2 atmosphere shows characteristic IR bands of ZIF-8. These results unveil that CZIF-matrix remains intact in CO_2 atmosphere but degrades back to ZIF-8 in N_2 atmosphere without CO_2 supplement during photocatalysis. The IR signals relating to MOC-16 (Figure 2B-g) become featureless in MOC-16@MOF samples due to low content of MOC-16, overwhelmed by strong vibrations of 2-MeIm and CO_3^{2-}.

In order to discern distribution of MOC-16 in heterogeneous photocatalysis, aberration corrected high-angle annular dark-field (HAADF) scanning transmission electron microscopy (STEM) imaging and energy-dispersive X-ray (EDX) spectroscopy element mapping were performed. Figure 3 gives representative HAADF-STEM images and element maps of MOC-16@ZIF-8 and MOC-16@CZIF. From the element distribution of MOC-16@ZIF-8, we can clearly see that both Ru and Pd atoms are homogenously scattered in ZIF-8 matrix (Figure 3g-h) with lower density than Zn, C and N elements (Figure 3b-c, 3f), which verifies that MOC-16 is uniformly encapsulated in the whole ZIF-8 matrix. Similar uniform distribution of Ru and Pd elements (Figure 3g'-h') in CZIF matrix is observed for MOC-16@CZIF. Therefore, the structural transformation from ZIF-8 to CZIF does not disturb the integrated MOC-16 in MOF-matrix. On the other hand, the obvious density-increase of O elements in MOC-16@CZIF (Figure 3d') in contrast to original MOC-16@ZIF-8 (Figure 3d) is evident, in accordance with appearance of CO_3^{2-} carbonate which is also homogenously dispersed in CZIF-matrix. However, after photocatalytic reaction under N_2 atmosphere, the recycled MOC-16@CZIF samples display morphology deterioration obviously (Figure S6), in agreement with the formation of ZnO/ZIF-8 conglomerates with much loose distribution of corresponding elements.

X-ray photoelectron spectroscopy (XPS) shown in Figure 4 were further carried out to monitor chemical states of Pd and Ru elements in heterogenous MOC@MOF before and after photocatalytic reaction, together with that of MOC-16 for comparison. The binding energy (BE) is calibrated to adventitious carbon C 1s peak at 284.8 eV, and summarized in Table S3. Although Ru 3d overlaps with C 1s in Figure 4A, Ru $3d_{5/2}$ at ~280.8 eV (Figure 4B) can be discerned in all samples, which is consistent with Ru^{2+} oxidation state.[31] Negligible variety of this peak in four samples indicates that

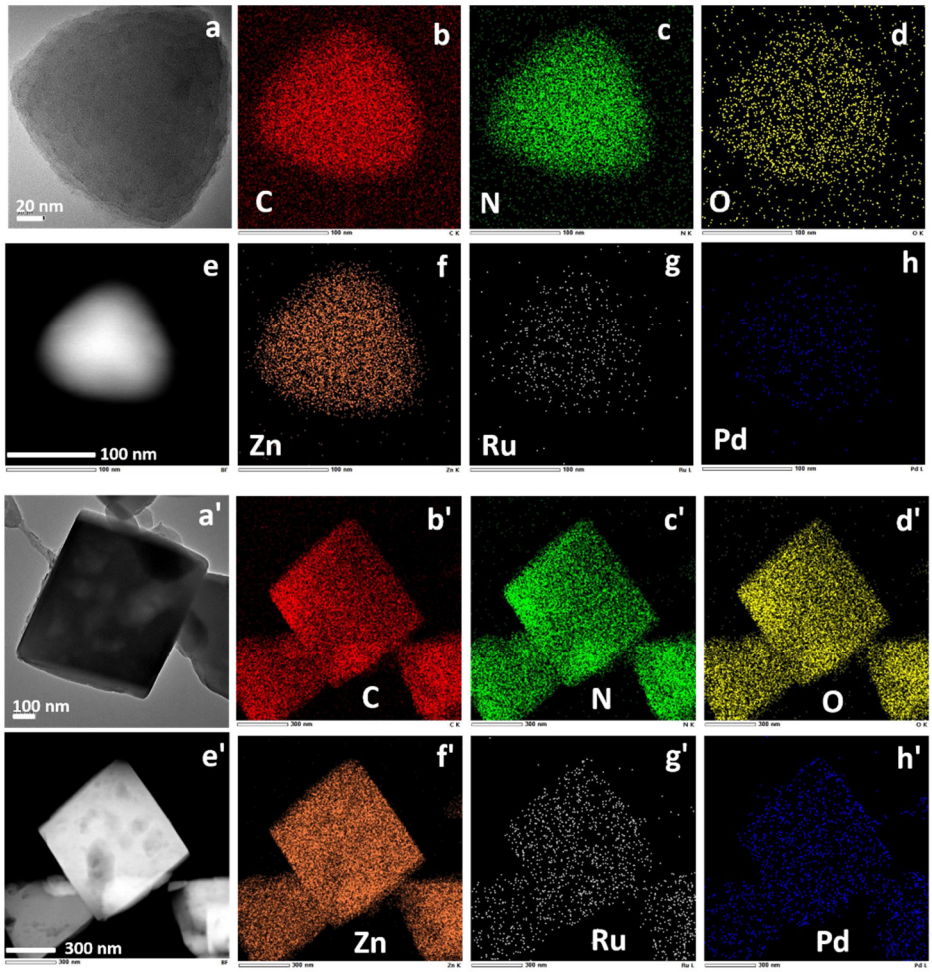

Figure 3. HAADF-STEM images (a, a', e, e') and corresponding elemental maps (b-d, b'-d', f-h, f'-h') of a-h) MOC-16@ZIF-8 and a'-h') MOC-16@CZIF.

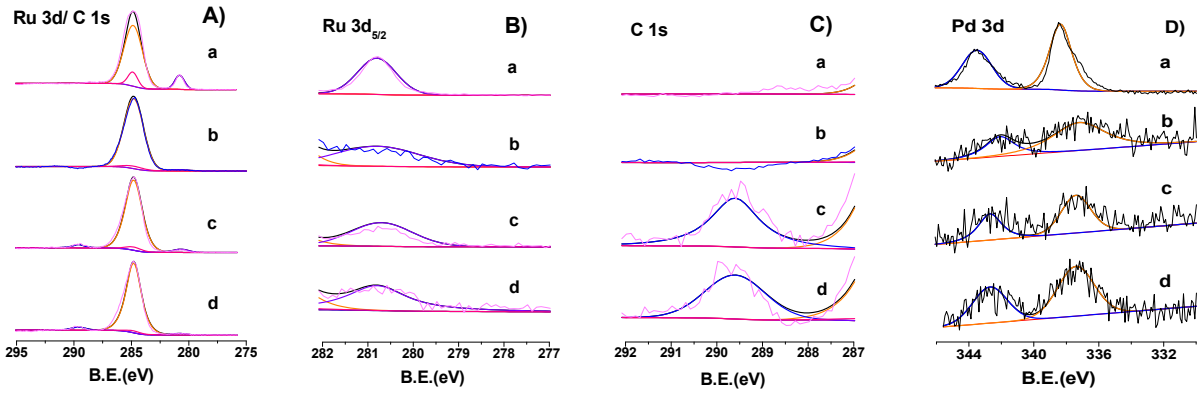

Figure 4. XPS spectra of A) Ru 3d/C 1s, B) Ru $3d_{5/2}$, C) C1s and D) Pd 3d in a) MOC-16, b) MOC-16@ZIF-8, c) MOC-16@CZIF and d) recycled MOC-16@CZIF under CO_2 atmosphere. Inset in A) is enlarged parts in regions of 282~278 and 292~288 eV.

Ru^{2+} oxidation state is sustained both in incorporation and photocatalysis processes. Additional peak of C 1s at 289.6 eV (Figure 4C) relating to CO_3^{2-} is observed in MOC-16@CZIF and recycled sample,[32] which further proves CO_3^{2-} nature in CZIF-matrix. In Figure 4D, double peaks of Pd corresponding to $3d_{5/2}$ and $3d_{3/2}$ are observed for all samples. When comparing binding energy, we can find that $3d_{5/2}$ peak is shifted from 338.4 to 337.4 eV when incorporating MOC-16 into matrix. It is still higher than binding energy of metallic Pd (~335 eV),[33] indicating that Pd^{2+} species is maintained. This 1 eV shift should relate to variation of chemical environment as MOC-16 is surrounded by CZIF-matrix.

Steady-state absorption and emission spectra are effective techniques to characterize electron structure of heterogenous MOC@MOF catalysts. As shown in Figure 5, the absorption spectra of MOC-16 in condensed state (Figure 5A) show two bands at about 280-350 and 400-550

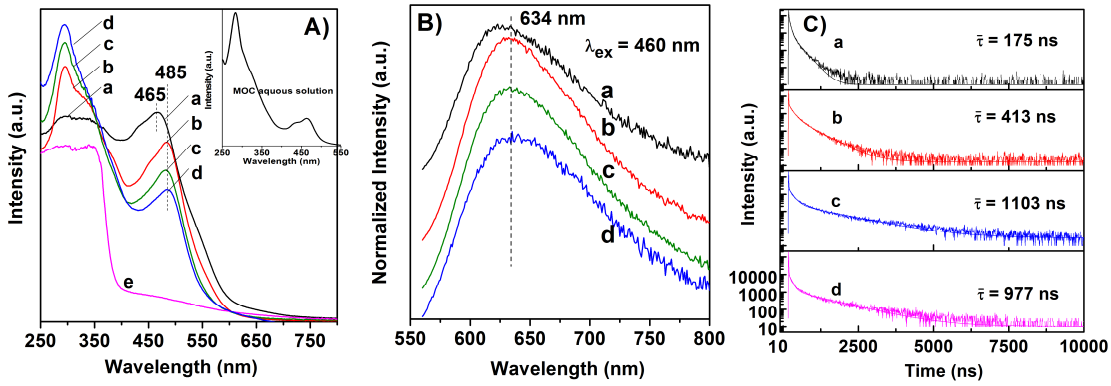

Figure 5. A) UV-visible absorption spectra, B) fluorescence spectra and C) time-resolved emission decay at 634 nm of a) MOC-16, b) MOC-16@ZIF-8, c) MOC-16@CZIF, d) recycled MOC-16@CZIF under CO_2 atmosphere, and e) recycled MOC-16@CZIF under N_2 atmosphere. Insert in A) shows UV-visible absorption spectrum of MOC-16 dissolved in H_2O solvent.

nm, originated from intra-ligand π-π* transition and metal-to-ligand charge transfer (^{1}MLCT of Phen←Ru), respectively.[5] When embedding MOC-16 into ZIF-8 matrix, the first band in UV region is narrowed around 290 nm and the second band in visible region is red-shifted from 465 to 485 nm, which is similar to spectra profile of MOC-16 dissolved in H_2O solvent (inset in Figure 5A). This may indicate that the encapsulation of MOC-16 into MOF-matrix is analogue to the dissolution of MOC-16 into solvent environment. For MOC-16@CZIF before and after photocatalytic reaction in CO_2 atmosphere, their absorption spectra are similar with those of MOC-16@ZIF-8. However, for the recycled MOC-16@CZIF after reaction in N_2 atmosphere, the characteristic bands of MOC-16 are replaced by a sharp band-edge absorption of ZnO at about 380 nm along with a tailing peak till 650 nm, in line with the structure degradation of MOC-16@CZIF to a mixture of ZnO and ZIF-8 as revealed by XRD result (Figure 2A-f). In the emission spectra (Figure 5B), a luminescence band centered around 634 nm, relating to $Ru(Phen)_3$-centred triplet ^{3}MLCT (metal-ligand charge transfer) state,[5] is observed for all three samples of MOC-16@ZIF-8, MOC-16@CZIF and recycled MOC-16@CZIF under CO_2 atmosphere. Compared with condensed state MOC-16, this band is red-shifted several nanometers due to the integration of MOC-16 into MOF-matrix. In contrast, the recycled MOC-16@CZIF under N_2 atmosphere displays no luminescence band in the same measurement condition. These absorption and emission spectral results indicate that incorporation of MOC-16 into MOF-matrix does not remarkably alter its ground-state spectroscopic property, only slightly perturbing the energy gap between the lowest excited-state and ground-state. For the recycled MOC-16@CZIF after reaction in N_2, disappearance of absorption and emission bands belonging to MOC-16 implies that, along with degradation of CZIF-matrix, the embedded MOC-16 is released from the matrix into solvent, which is in accordance with a color change from original orange to nearly gray (Figure S7). This observation accounts for the reason that photocatalytic activity of MOC-16@CZIF is dramatically decreased after the first cycle under N_2 atmosphere (Figure 1B).

To understand how the high efficiency of MOC-16 as a PMD with multichannel directional electron transfer[5] is influenced by the MOF-matrix owing to the structural and spatial heterogeneity underlying the interface between MOC-16 and MOF-matrix, the multi-step-relaxation processes of MOC-16, involving intersystem crossing (ISC) from ^{1}MLCT to ^{3}MLCT, intraligand charge-transfer (ILCT), ligand-to-metal charge-transfer (LMCT), were investigated by femtosecond transient absorption spectra (Figure S8). The transient absorption of MOC-16@ZIF-8 features in a broad excited-state absorption (ESA) in 530–730 nm region accompanied by a ground-state bleaching (GSB) centered around 490 nm, resembling that of MOC-16 dissolved in DMSO.[5] For MOC-16@CZIF, a similar GSB profile centered at 490 nm is observed. The characteristic time constants of both MOC-16@ZIF-8 and MOC-16@CZIF obtained through a global analysis are summarized in Table S4. It is clear that the ISC and ILCT processes occur in a comparable picoseconds time scale with that of MOC-16, although the following LMCT process is slightly sluggish than MOC-16 (535, 630 *vs.* 122 ps). These results reveal that the dynamics of electron transfer in picosecond domain is not significantly affected when MOC-16 is encapsulated in MOF-matrix, in consistent with the steady-state absorption and emission spectral measurements. Therefore, the efficient and multichannel directional electron transfer from the photosensitizing centers to catalytic centers, characteristic of MOC-type PMD, are well inherited for MOC-16@MOF. On the contrary, the triplet excited-state in nanosecond domain is found to be extremely sensitive to MOF-matrix. Figure 5C shows emission decay curves monitored at maximum emission wavelength, which are analyzed by double exponential fitting to average lifetimes (Table S5). It turns out that encapsulating MOC-16 into ZIF-8 matrix causes an increase of the average lifetime relating to excited ^{3}MLCT state from 175 to 413 ns. When transforming matrix structure from ZIF-8 to carbonate CZIF, a further increase to 1103 ns is achieved. Similar prolonging emission lifetime of ^{3}MLCT state was also observed by Lin et al. when doping $[Ir^{III}(ppy)_2(bpy)]^+$ into rigid MOF framework.[19] In our case, significant elongation of lifetime may be attributable to inhibition of the non-radiative vibrational relaxation, a competing loss channel with radiative luminescence from ^{3}MLCT excited-state to ground state, after incorporating MOC-16 into the rigid MOF-matrix. Transformation of ZIF-8 matrix to carbonate CZIF may further consolidate MOC-16 owing to stronger coordination between Zn^{2+} and CO_3^{2-} anions, thus the long-lived ^{3}MLCT excited states consequently benefits the photocatalytic process owing to MOC-16 heterogenization.

Another important factor to influence the proton reduction by heterogeneous catalyst is the capability of proton conductivity, as we know, in nature, precisely controlled delivery of protons is critical in hydrogenase enzymes that catalyze H_2 production.[34] ZIF-8 is well known hydrophobic, [35-37,38] thereof unfavorable to H_2 generation. However, when transformed to carbonate CZIF, the MOF-matrix is expected to turn hydrophilic. This is testified by the static contact angle measurements of the surface wettability (Figure S9). MOC-16@ZIF-8 shows strong hydrophobicity with a contact angle of ~139°. By contrast, MOC-16@CZIF is totally water-wettable with zero contact angle (Figure S9), evidently due to its carbonate nature. It was also reported that aquo- and hydroxo-rich MOF nodes could act as proton-relaying to facilitate local proton delivery and/or long-range proton transport.[39] Based on the superhydrophilic feature, it is supposed that CO_3^{2-} in CZIF-matrix may function as proton relay to manipulate the local chemical environment of confined MOC-16, and guarantees sufficient proximity between proton and catalytic sites to interact with each other for chemical reactions. This may be the pivot point explaining why hydrophobic ZIF-8 matrix does not work on H_2 evolution but CZIF-matrix is efficient.

In order to explore the role of H_2O molecules in photocatalysis, several control experiments with different solvents were performed and summarized in Table S1. In the absence of H_2O, only trace H_2 is detected (entries 7 and 8) with BIH as sacrificial agent under both N_2 and CO_2 atmosphere, which suggests that H_2O is indispensable for H_2 generation. Considering the wettability of CZIF-matrix, it is speculated that water serves as proton carriers to construct hydrogen bonded networks for proton transfer. Further evidence comes from the control experiment utilizing pure H_2O as photocatalytic media, where BIH is undissolved and emulsified together with MOC-16@CZIF catalyst. H_2 evolution is still detected under CO_2 atmosphere (entry 9) but minimized under N_2 atmosphere (entry 10). Taking the CZIF-matrix degradation in absence of CO_2 feeding into consideration, it is deduced that protons transfer stems from formation of aqueous carbonic acid under CO_2 atmosphere. Considering the pH value of reaction solution is approximate to 6 under CO_2 atmosphere, another control experiment under N_2 atmosphere is carried out to clarify the pH effect, where solution pH is adjusted by acetic acid to 6 with other conditions equivalent. A significantly low H_2 evolution is detected (entry 11), revealing the imperative role of CO_2 for protons transfer beyond pH regulation. It is worthy of noting that, acid conditions except for CO_2 mediation will cause dissociation of CZIF-matrix.

In addition to proton transfer, electrical conductivity is also important for heterogeneous photocatalysis concerning electron mobility. The linear I-V characteristics of MOC-16@ZIF-8 exhibits conductivity at the magnitude of $\sim 10^{-10}$ S/cm, comparable with that of MOC-16@CZIF (Figure S10, Table S6). Interestingly, when infiltrating sacrificial agent of BIH onto heterogeneous MOC-16@MOF catalysts, the current is significantly enhanced with conductivity increasing by one order of magnitude to $\sim 10^{-9}$ S/cm, of which MOC-16@CZIF displays triple-fold conductivity compared with MOC-16@ZIF-8 (3.23×10^{-9} *vs.* 1.06×10^{-9} S/cm). It had been reported that the redox-active guest molecules are effective to improve conductivity of a host material.[40,41] In this case, BIH may behave as an electron donor with sufficient reducing power in solution and solid state, thus inducing free charge carriers within heterogenous MOC-16@MOF catalysts *via* charge-transfer interaction to promote conductivity.

CONCLUSIONS

In summary, an MOC-16 based PMD with well-organized multiple photosensitizers and catalyzers has been successfully incorporated into an MOF-matrix via a coordination-assisted secondary assembly process followed by in-situ transformation into carbonate CZIF-matrix. The rigid CZIF-matrix isolates MOC-16 PMDs from each other in coordination interspace while maintaining their effective photophysical and photochemical features. This heterogenized MOC-16@CZIF photocatalyst can survive in ambient reaction condition in the presence of H_2O and CO_2, preventing catalyst from deactivation and degradation. Moreover, synergistic effect is endowed for such MOC@MOF via structural hetereogenity, which renders long-lived excited-state electron in MOC-16 to microsecond order of magnitude. The hydrophilic character of CO_3^{2-} in CZIF-matrix assists in proton delivery to proximal catalytic sites, utilizing H_2O as proton carriers. The local electron mobility is also boosted by reducing BIH acting as charge carriers, favorable for efficient H_2 production. Therefore, the integrated MOC-16@CZIF photocatalyst in this work presents a unique example to combine homogeneous PMDs with MOF-derived materials, giving rise to a heterogenization approach to incorporate molecular catalysts into MOF-matrix to engender appropriate microenvironment to mimic structural and functional features of nature photosystem, and circumvent the intrinsic vulnerability of molecular photocatalyts to achieve efficient and practical photo-conversion.

EXPERIMENTAL SECTION

Synthesis of MOC-16@ZIF-8: Sample was prepared by a procedure similar to that described for ZIF-8. The encapsulation of MOC-16 into ZIF-8 matrix was carried out by mixing a certain volume of pristine MOC-16 solution with 100 μL $Zn(NO_3)_2$ aqueous solution (0.01462 g , 0.05 mol/L). After ultrasonic dispersion for 30 min, the mixture was rapidly injected into 1 mL MeIm aqueous solution (0.2838 g, 3.5 mol/L) with a molar ratio of Zn^{2+} to MeIm being 1:70 under vigorous stirring. After a 30 min reaction, the resulting precipitate was centrifuged, washed, and vacuum dried at 50 °C to get orange powder.

Synthesis of MOC-16@CZIF: 200 mg MOC-16@ZIF-8 powder was dispersed in 1.5 mL deionized (DI) water under vigorous stirring, then sealing into a 40 mL glass vial with bubbling CO_2 continuously. After stirring for 2 h at room temperature, the product was collected by centrifuging, washed with DMSO, MeCN and DI water for several times, and then vacuum dried at 65 °C for 48 h. CZIF was obtained in a similar way. The noble metal contents of Pd and Ru were quantitated with inductively coupled plasma-atomic emission spectrometry (ICP-AES) as 0.03 and 0.04 wt%, respectively.

Photocatalytic proton reduction: Hydrogen production experiments were carried out using a 40 mL closed glass

vial with magnetic stirring. The amount of produced H_2 was analyzed using an off-line gas chromatography (FuLi Analytical Instrument Co., Ltd, GC9790 plus) equipped with a thermal conductivity detector and a N_2 carrier. Typically, 1 mg powder sample was suspended in 5 mL mixed solvent of H_2O and MeCN (v/v = 2/3) in the presence of 14 mg sacrificial agent of 1,3-dimethyl-2-phenyl-2,3-dihydro-1H-benzimidazole (BIH). The light source was a 300 W Xe lamp (PLS-SXE-300C, Beijing Perfect light) supplying the visible light ($\lambda > 420$ nm) by using a 420 nm cut-off filter. In recycle experiment, BIH solid powder was directly added into the previous reaction solution to restart the following cycles.

Transient absorption measurement: It was performed by equipping a regeneratively amplified Ti:Sapphire laser source (Coherent Legend, 800 nm, 150 fs, 5 mJ per pulse, and 1 kHz repetition rate) and Helios (Ultrafast Systems LLC) spectrometers. Portion of the 800 nm output (75%) pulse was frequency-doubled in a BaB_2O_4 (BBO) crystal, which could generate 400 nm pump light, meanwhile the remaining portion of the output was concentrated into a sapphire window to produce white light continuum (420-780 nm) probe light. The 400 nm pump beam was formed from part of the 800 nm output pulse from the amplifier and its power was adjusted by a range of neutral-density filters. The pump beam was focused at the sample with a beam waist of about ~360 μm and the power intensity was fixed at 14 μJ cm^{-2}. A mechanical chopper was employed to modulate the pump repetition frequency to 1/2 the probe repetition rate. The probe pulse was recorded using a fiber optics-coupled multichannel spectrometer and the optical path in samples was 5 mm.

ASSOCIATED CONTENT

Supporting Information

The Supporting Information is available free of charge on the ACS Publications website. Experimental details, materials characterization, supplementary data.

AUTHOR INFORMATION

Corresponding Authors

*shijying@mail.sysu.edu.cn
*cesscy@mail.sysu.edu.cn

Notes

The authors declare no competing financial interest.

ACKNOWLEDGEMENTS

We gratefully acknowledge the financial support from the NSFC Project (21875293, 21821003, 21890380, 21720102007), Local Innovative and Research Teams Project of Guangdong Pearl River Talents Program (2017BT01C161), the NSF of Guangdong Province (2016A030313268), the STP Project of Guangzhou (201804010386) and the Fundamental Research Funds for the Central Universities (17lgzd18). We thank V. Lukyanchenko for assistance with TA data collection.

REFERENCES

(1) Zhang, B.; Sun, L. Artificial photosynthesis: opportunities and challenges of molecular catalysts. *Chemical Society Reviews* **2019**, *48*, 2216-2264.

(2) Guo, S.; Chen, K.-K.; Dong, R.; Zhang, Z.-M.; Zhao, J.; Lu, T.-B. Robust and Long-Lived Excited State Ru(II) Polyimine Photosensitizers Boost Hydrogen Production. *ACS Catalysis* **2018**, *8*, 8659-8670.

(3) Shi, J.; Cui, H. n.; Liang, Z.; Lu, X.; Tong, Y.; Su, C.; Liu, H. The roles of defect states in photoelectric and photocatalytic processes for ZnxCd1-xS. *Energy & Environmental Science* **2011**, *4*, 466-470.

(4) Manbeck, G. F.; Fujita, E.; Brewer, K. J. Tetra- and Heptametallic Ru(II),Rh(III) Supramolecular Hydrogen Production Photocatalysts. *Journal of the American Chemical Society* **2017**, *139*, 7843-7854.

(5) Chen, S.; Li, K.; Zhao, F.; Zhang, L.; Pan, M.; Fan, Y.-Z.; Guo, J.; Shi, J.; Su, C.-Y. A metal-organic cage incorporating multiple light harvesting and catalytic centres for photochemical hydrogen production. *Nature Communications* **2016**, *7*.

(6) Balzani, V. Photochemical molecular devices. *Photochemical & Photobiological Sciences* **2003**, *2*, 459-476.

(7) Ozawa, H.; Sakai, K. Photo-hydrogen-evolving molecular devices driving visible-light-induced water reduction into molecular hydrogen: structure-activity relationship and reaction mechanism. *Chemical Communications* **2011**, *47*, 2227-2242.

(8) Pfeffer, M. G.; Schaefer, B.; Smolentsev, G.; Uhlig, J.; Nazarenko, E.; Guthmuller, J.; Kuhnt, C.; Waechtler, M.; Dietzek, B.; Sundstroem, V.; Rau, S. Palladium versus Platinum: The Metal in the Catalytic Center of a Molecular Photocatalyst Determines the Mechanism of the Hydrogen Production with Visible Light. *Angewandte Chemie-International Edition* **2015**, *54*, 5044-5048.

(9) Li, K.; Zhang, L.-Y.; Yan, C.; Wei, S.-C.; Pan, M.; Zhang, L.; Su, C.-Y. Stepwise Assembly of Pd-6(RuL3)(8) Nanoscale Rhombododecahedral Metal-Organic Cages via Metalloligand Strategy for Guest Trapping and Protection. *Journal of the American Chemical Society* **2014**, *136*, 4456-4459.

(10) Zeng, L.; Guo, X.; He, C.; Duan, C. Metal–Organic Frameworks: Versatile Materials for Heterogeneous Photocatalysis. *ACS Catalysis* **2016**, *6*, 7935-7947.

(11) Wang, S.; Wang, X. Multifunctional Metal–Organic Frameworks for Photocatalysis. *Small* **2015**, *11*, 3097-3112.

(12) Liu, J.; Chen, L.; Cui, H.; Zhang, J.; Zhang, L.; Su, C.-Y. Applications of metal–organic frameworks in heterogeneous supramolecular catalysis. *Chemical Society Reviews* **2014**, *43*, 6011-6061.

(13) Zhou, T.; Du, Y.; Borgna, A.; Hong, J.; Wang, Y.; Han, J.; Zhang, W.; Xu, R. Post-synthesis modification of a metal–organic framework to construct a bifunctional photocatalyst for hydrogen production. *Energy & Environmental Science* **2013**, *6*, 3229-3234.

(14) Nepal, B.; Das, S. Sustained Water Oxidation by a Catalyst Cage-Isolated in a Metal–Organic Framework. *Angewandte Chemie International Edition* **2013**, *52*, 7224-7227.

(15) Wang, C.; Xie, Z.; deKrafft, K. E.; Lin, W. Doping Metal–Organic Frameworks for Water Oxidation, Carbon Dioxide Reduction, and Organic Photocatalysis. *Journal of the American Chemical Society* **2011**, *133*, 13445-13454.

(16) Pullen, S.; Fei, H.; Orthaber, A.; Cohen, S. M.; Ott, S. Enhanced Photochemical Hydrogen Production by a Molecular Diiron Catalyst Incorporated into a Metal–Organic Framework. *Journal of the American Chemical Society* **2013**, *135*, 16997-17003.

(17) Fei, H.; Sampson, M. D.; Lee, Y.; Kubiak, C. P.; Cohen, S. M. Photocatalytic CO2 Reduction to Formate Using a Mn(I) Molecular Catalyst in a Robust Metal–Organic Framework. *Inorganic Chemistry* **2015**, *54*, 6821-6828.

(18) Nasalevich, M. A.; Becker, R.; Ramos-Fernandez, E. V.; Castellanos, S.; Veber, S. L.; Fedin, M. V.; Kapteijn, F.; Reek, J. N. H.; van der Vlugt, J. I.; Gascon, J. Co@NH2-MIL-125(Ti): cobaloxime-derived metal–organic framework-based composite for light-driven H2 production. *Energy & Environmental Science* **2015**, *8*, 364-375.

(19) Wang, C.; deKrafft, K. E.; Lin, W. Pt Nanoparticles@Photoactive Metal–Organic Frameworks: Efficient Hydrogen Evolution via Synergistic Photoexcitation and Electron Injection. *Journal of the American Chemical Society* **2012**, *134*, 7211-7214.

(20) Kim, D.; Whang, D. R.; Park, S. Y. Self-Healing of Molecular Catalyst and Photosensitizer on Metal–Organic Framework: Robust Molecular System for Photocatalytic H2

Evolution from Water. *Journal of the American Chemical Society* **2016**, *138*, 8698-8701.

(21) Sasan, K.; Lin, Q.; Mao, C.; Feng, P. Incorporation of iron hydrogenase active sites into a highly stable metal–organic framework for photocatalytic hydrogen generation. *Chemical Communications* **2014**, *50*, 10390-10393.

(22) Lan, G.; Zhu, Y.-Y.; Veroneau, S. S.; Xu, Z.; Micheroni, D.; Lin, W. Electron Injection from Photoexcited Metal–Organic Framework Ligands to Ru_2 Secondary Building Units for Visible-Light-Driven Hydrogen Evolution. *Journal of the American Chemical Society* **2018**, *140*, 5326-5329.

(23) Majewski, M. B.; Peters, A. W.; Wasielewski, M. R.; Hupp, J. T.; Farha, O. K. Metal–Organic Frameworks as Platform Materials for Solar Fuels Catalysis. *ACS Energy Letters* **2018**, *3*, 598-611.

(24) Lee, Y.; Kim, S.; Kang, J. K.; Cohen, S. M. Photocatalytic CO2 reduction by a mixed metal (Zr/Ti), mixed ligand metal–organic framework under visible light irradiation. *Chemical Communications* **2015**, *51*, 5735-5738.

(25) Luo, Y.; Fan, S.; Yu, W.; Wu, Z.; Cullen, D. A.; Liang, C.; Shi, J.; Su, C. Fabrication of Au-25(SG)(18)-ZIF-8 Nanocomposites: A Facile Strategy to Position Au-25(SG)(18) Nanoclusters Inside and Outside ZIF-8. *Advanced Materials* **2018**, *30*.

(26) Li, L.; Xiang, S. L.; Cao, S. Q.; Zhang, J. Y.; Ouyang, G. F.; Chen, L. P.; Su, C. Y. A synthetic route to ultralight hierarchically micro/mesoporous Al(III)-carboxylate metal-organic aerogels. *Nature Communications* **2013**, *4*, 9.

(27) Tsuruoka, T.; Furukawa, S.; Takashima, Y.; Yoshida, K.; Isoda, S.; Kitagawa, S. Nanoporous Nanorods Fabricated by Coordination Modulation and Oriented Attachment Growth. *Angewandte Chemie International Edition* **2009**, *48*, 4739-4743.

(28) Mottillo, C.; Friščić, T. Carbon Dioxide Sensitivity of Zeolitic Imidazolate Frameworks. *Angewandte Chemie International Edition* **2014**, *53*, 7471-7474.

(29) Park, K. S.; Ni, Z.; Cote, A. P.; Choi, J. Y.; Huang, R.; Uribe-Romo, F. J.; Chae, H. K.; O'Keeffe, M.; Yaghi, O. M. Exceptional chemical and thermal stability of zeolitic imidazolate frameworks. *Proceedings of the National Academy of Sciences of the United States of America* **2006**, *103*, 10186-10191.

(30) Huang, X. C.; Lin, Y. Y.; Zhang, J. P.; Chen, X. M. Ligand-directed strategy for zeolite-type metal-organic frameworks: zinc(II) imidazolates with unusual zeolitic topologies. *Angewandte Chemie* **2006**, *45*, 1557-1559.

(31) Morgan, D. J. Resolving ruthenium: XPS studies of common ruthenium materials. *Surface and Interface Analysis* **2015**, *47*, 1072-1079.

(32) Shchukarev, A. V.; Korolkov, D. V. XPS Study of group IA carbonates. *Central European Journal of Chemistry* **2004**, *2*, 347-362.

(33) Arrigo, R.; Schuster, M. E.; Xie, Z.; Yi, Y.; Wowsnick, G.; Sun, L. L.; Hermann, K. E.; Friedrich, M.; Kast, P.; Hävecker, M.; Knop-Gericke, A.; Schlögl, R. Nature of the N–Pd Interaction in Nitrogen-Doped Carbon Nanotube Catalysts. *ACS Catalysis* **2015**, *5*, 2740-2753.

(34) Helm, M. L.; Stewart, M. P.; Bullock, R. M.; DuBois, M. R.; DuBois, D. L. A Synthetic Nickel Electrocatalyst with a Turnover Frequency Above 100,000 s^{−1} for H₂ Production. *Science* **2011**, *333*, 863-866.

(35) Sann, E. E.; Pan, Y.; Gao, Z.; Zhan, S.; Xia, F. Highly hydrophobic ZIF-8 particles and application for oil-water separation. *Separation and Purification Technology* **2018**, *206*, 186-191.

(36) Zhang, K.; Lively, R. P.; Dose, M. E.; Brown, A. J.; Zhang, C.; Chung, J.; Nair, S.; Koros, W. J.; Chance, R. R. Alcohol and water adsorption in zeolitic imidazolate frameworks. *Chemical Communications* **2013**, *49*, 3245-3247.

(37) Küsgens, P.; Rose, M.; Senkovska, I.; Fröde, H.; Henschel, A.; Siegle, S.; Kaskel, S. Characterization of metal-organic frameworks by water adsorption. *Microporous and Mesoporous Materials* **2009**, *120*, 325-330.

(38) Ortiz, A. U.; Freitas, A. P.; Boutin, A.; Fuchs, A. H.; Coudert, F.-X. What makes zeolitic imidazolate frameworks hydrophobic or hydrophilic? The impact of geometry and functionalization on water adsorption. *Physical Chemistry Chemical Physics* **2014**, *16*, 9940-9949.

(39) Hod, I.; Deria, P.; Bury, W.; Mondloch, J. E.; Kung, C.-W.; So, M.; Sampson, M. D.; Peters, A. W.; Kubiak, C. P.; Farha, O. K.; Hupp, J. T. A porous proton-relaying metal-organic framework material that accelerates electrochemical hydrogen evolution. *Nature Communications* **2015**, *6*, 8304.

(40) Talin, A. A.; Centrone, A.; Ford, A. C.; Foster, M. E.; Stavila, V.; Haney, P.; Kinney, R. A.; Szalai, V.; El Gabaly, F.; Yoon, H. P.; Léonard, F.; Allendorf, M. D. Tunable Electrical Conductivity in Metal-Organic Framework Thin-Film Devices. *Science* **2014**, *343*, 66-69.

(41) Sun, L.; Campbell, M. G.; Dincă, M. Electrically Conductive Porous Metal – Organic Frameworks. *Angewandte Chemie International Edition* **2016**, *55*, 3566-3579.

Table of Contents